nature astronomy

Article

https://doi.org/10.1038/s41550-023-01945-7

JWST/NIRCam detections of dusty subsolar-mass young stellar objects in the Small Magellanic Cloud

Received: 19 December 2022

Accepted: 15 March 2023

Published online: 24 April 2023

Check for updates

Olivia C. Jones[1] ✉, Conor Nally[2], Nolan Habel[3], Laura Lenkić[3], Katja Fahrion[4], Alec S. Hirschauer[5], Laurie E. U. Chu[6], Margaret Meixner[3], Guido De Marchi[4], Omnarayani Nayak[5], Massimo Robberto[5,7], Elena Sabbi[5], Peter Zeidler[8], Catarina Alves de Oliveira[9], Tracy Beck[5], Katia Biazzo[10], Bernhard Brandl[11], Giovanna Giardino[4], Teresa Jerabkova[12], Charles Keyes[5], James Muzerolle[5], Nino Panagia[5], Klaus Pontoppidan[5], Ciaran Rogers[11], B. A. Sargent[5,7] & David Soderblom[5]

Low-mass stars are the most numerous stellar objects in the Universe. Before the James Webb Space Telescope (JWST), we had limited knowledge of how planetary systems around low-mass stars could form at subsolar metallicities. Here we present JWST observations of NGC 346, a star-forming region in the metal-poor Small Magellanic Cloud, revealing a substantial population of subsolar-mass young stellar objects (YSOs) with an infrared excess. We notice that continuing low-mass star formation is concentrated along dust filaments. We detected roughly 500 YSOs and pre-main-sequence (PMS) stars from more than 45,000 unique sources, using all four NIRCam wide filters with deep, high-resolution imaging. From these observations, we construct detailed near-infrared colour–magnitude diagrams with which preliminary categorizations of YSO classes are made. For the youngest, most deeply embedded objects, JWST/NIRCam is ten magnitudes more sensitive than Spitzer observations at comparable wavelengths, and reaches two magnitudes fainter than Hubble Space Telescope for more evolved PMS sources, corresponding to roughly 0.1 $M_{\odot}$. The infrared sensitivity and resolution of JWST allows us to detect embedded low-mass star formation in an extragalactic environment. Furthermore, evidence of infrared excesses and accretion suggests that the dust required for rocky planet formation is present at metallicities as low as 0.2 $Z_{\odot}$, which are akin to those in place at cosmic noon.

Located in the Small Magellanic Cloud (SMC) at a distance of roughly 62 kpc (ref. 1), NGC 346 is a prominent young cluster (roughly 3 million years (Myr)[2]) of actively forming stars. It is the brightest and largest star-formation region in this metal-poor galaxy (roughly 1/5 $Z_{\odot}$; ref. 3) that has a comparable metallicity to galaxies at the epoch of peak star formation 'cosmic noon' (refs. 4,5). Below these levels of chemical enrichment, the dust content of the interstellar medium drops precipitously, altering the environment in which stars form (for example, refs. 6,7).

A full list of affiliations appears at the end of the paper. ✉e-mail: olivia.jones@stfc.ac.uk

It is unknown whether sufficient quantities of dust survive the star-formation process to contribute to the formation of rocky planetary systems in low-metallicity environments. Below a certain threshold of metal abundance, planetesimal formation via the streaming instability is suppressed[8,9]. The metallicity of inner protoplanetary discs is therefore thought to play a critical role in the ability to form terrestrial planets. Further, the dust content of discs sets their lifetimes as lower-metallicity systems are more susceptible to fast photo-evaporation[10]. It is therefore of great interest to identify low-mass young stellar objects (YSOs) and discern their dust content.

The star-formation history of NGC 346 is complex, with multiple stellar populations identified within the cluster, for example, ref. 11. Powering the ionization of this giant H II region are more than 30 spectroscopically identified massive (35–100 $M_{\odot}$) O-type stars[12–14], the largest such sample in the SMC, which dominate the radiative and mechanical feedback. Deep Hubble Space Telescope (HST) images reveal thousands of low-mass (0.6–3 $M_{\odot}$) pre-main-sequence (PMS) stars[15], which are distributed throughout the nebula and are connected by gas and dust filaments[16–18]. Spitzer and Herschel surveys of the SMC[19–21] unveiled approximately 100 candidate YSOs in the very early stages of formation within the NGC 346 complex[22–24]. These high-mass YSOs possess typical masses of 8 $M_{\odot}$ and have formed within roughly the past 1 Myr. They are located at the edge of or inside dusty pillars, which are often associated with Hα emission. Their presence establishes that star formation is ongoing throughout the complex at a rate of more than 3.2×10^{-3} $M_{\odot}$ yr^{-1} (ref. 22). In the infrared, spectroscopic data for the young populations in NGC 346 are limited. Spitzer infrared spectrograph data spectroscopically confirmed the identity of six massive YSOs in the cluster[25]. Reference 26 obtained HK band spectra to confirm the existence of three early-type stars in NGC 346. Most recently, ref. 27 used VLT/KMOS to observe roughly 15 other YSO candidates that were resolved into multiple young stars still accreting mass.

Overall, NGC 346 possesses a complex distribution of hierarchically linked star clusters of varying ages that inhabit a variety of environments[28], and which are dispersed across the extended field[17,29,30]. Within the interstellar medium, there is a wide range of substructures exhibited in polycyclic aromatic hydrocarbon emission (PAH) (8 µm), warm dust (24 µm) and molecular gas CO $J = 2–1$ (refs. 28,31,32). A tight correlation is seen between the molecular gas, 8 µm emission and Hα, which presents as a well-defined bar extending from the centre of the region to the northeast and as an arc structure extending from southeast to northwest. A recent Atacama Large Millimeter/Submillimeter Array (ALMA) CO($J = 1–0$) study[33] discovered that the intersection of three colliding clumpy filaments is cospatial with the locations of a cluster of YSOs and PMS stars. Using HST proper motions and VLT and MUSE radial velocities, refs. 34 and 35 showed that stars in NGC 346 move along a wide spiral and that clusters of YSOs and young PMS stars seem to be predominately located where the coherent motion field shows significant changes, hence turbulence is still driving star formation across the system.

NGC 346 is one of the most active star-forming regions in the Local Group. Its proximity, size (roughly 100×100 pc^2), low foreground extinction and an abundance of wide-field, high-resolution panchromatic data make it an ideal system for the study of both low- and high-mass star formation, the effects of this star formation on the surrounding medium and the potential triggers of star formation in an environment vastly different from our local galactic surroundings, and akin to galaxies at cosmic noon.

Results and discussion

Images

We observed NGC 346 with JWST, using the Near Infrared Camera (NIRCam[36]) F115W, F187N, F200W, F277W, F335M and F444W filters. The NIRCam images of NGC 346 shown in Fig. 1 reveal the complex filamentary structure of the NGC 346 main arc, dominated by emission from warm dust and PAHs, together with the intermediate-age BS90 cluster[37] just above the centre. The brightest red stars are located along dust ridges, in tips of warm dust lanes, in large subclusters within the centre NGC 346 arc or in smaller clumps located along the main arc and northeast perpendicular filament. The images show large variations in the dust morphology and highlight feedback from the complex star-formation history of the region. The impact of star formation and stellar feedback is revealed by the heating of the dust and fluorescing PAHs due to C–H bond stretching in the F335M band[38,39,40]. This occurs on the edges of the main arc structure illuminated by ultraviolet photons from massive stars compared to the surrounding roughly $T = 600$ K dust seen in the F444W band. The northeast filament perpendicular to the NGC 346 main body extends further than what is seen in HST data and is brightest in the F335M band.

Identification of YSOs

As they are enshrouded in collapsing dusty envelopes and accretion discs[41–43], young YSOs are best identified using infrared colours. As they evolve and the circumstellar envelopes and discs dissipate, the central star becomes more apparent in shorter-wavelength light. From our initial band-matched photometric catalogue, 45,583 unique point sources were detected in all four of our wide-band NIRCam filters. This selection provides the most reliable colour–magnitude diagrams (CMDs) at the cost of some additional photometric depth.

CMDs constructed from the galactic extinction-corrected photometry are presented in Fig. 2. The details of the aperture photometry and corrections are given in the section on Photometry. In these near-infrared CMDs, the populations of red giant branch (RGB), red clump and upper main-sequence (UMS) stars are clearly separated from the dominant population of lower main-sequence and PMS stars. Table 1 lists the colour selection criteria for these populations and the number of sources in each class. Only JWST–NIRCam data were used in these classifications. Evolved stars (for example, red supergiants, asymptotic giant branch and postasymptotic giant branch stars) are brighter than the saturation limit and thus not expected to appear in this CMD. Furthermore, as NIRCam (point spread function of roughly 0.1 arcsec) resolves structures for distant galaxies, contamination from background galaxies and extended sources is negligible in our point-source catalogue and corresponding CMDs.

The F115W filter is essential to the identification of UMS, red clump and RGB stars, as these sequences, as well as main-sequence turn-off stars, are conflated in CMDs using longer-wavelength colours. In our CMDs, elevated photometric uncertainties cause scatter for sources near our detection limit, whereas a spread of ages and differential extinction across the field broadens the shape of the evolutionary sequences at all magnitudes. To visualize the effect of extinction, we show on the diagrams the reddening vector corresponding to a total extinction of $A_V = 5$ according to the SMC Bar Average Extinction Curve of ref. 44.

When compared to optical CMDs derived from HST data, we find more than 6,000 sources that are consistent with PMS stars in the mass range between roughly 0.5 and 4 $M_{\odot}$ on the basis of their colours and magnitudes[15,16]. Furthermore, we find candidate PMS stars in F115W extending at least two magnitudes below the HST detection limit, suggesting that we can observe T-Tauri stars down to roughly 0.1 $M_{\odot}$. Reference 18 used Hα excess to identify bona fide PMS with active accretion. Of these PMS candidates, 435 have a match in the NIRCam point-source catalogue, we refer to these sources as HST-PMS in the figures.

To disentangle young stars (less than 10 Myr) from other populations in the field, we use an F200W–F444W versus F115W–F187N colour–colour diagram (2CD, Fig. 2). Narrow-band photometry with the F187N filter traces the hydrogen Paα recombination line at 1.875 µm, characteristic of young PMS stars undergoing mass accretion. Approximately 8,500 sources are reliably detected in F187N. When this can be unambiguously identified, the accretion luminosity and mass accretion

https://doi.org/10.1038/s41550-023-01945-7

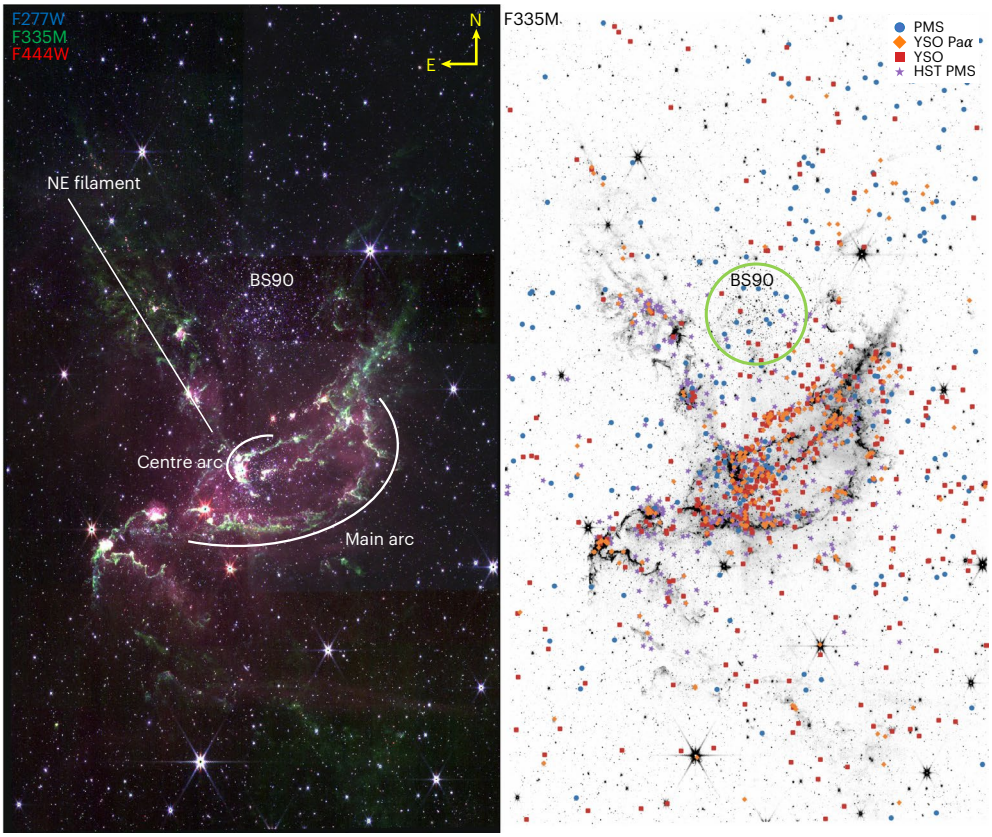


Fig. 1 | NIRCam mosaics of NGC 346. The left panel shows a three-colour composite mosaic of NGC 346 combining the F277W (blue), F335M (green) and F444W (red) filters. The region is rich in structures of knots, arcs and filaments. Areas of bright pink and/or red emission are associated with clumpy star formation. The spatially resolved PAH emission excited by ultraviolet photons in green is brightest in regions corresponding to the edges of dense material, characteristic of a photodissociation region. Massive stars, stars belonging to the BS90 cluster (circled in green) and the SMC field population are also visible. The right panel shows a mosaic image from the F335M filter showing four different populations of stars (Fig. 2): PMS stars (blue circles), YSOs with Paα (orange diamonds), YSOs without Paα (red squares) and stars matched with the HST-PMS catalogue (purple stars).

rate can be derived following methods similar to that developed by ref. 45 using Hα.

The F200W–F444W versus F115W–F187N 2CD shows a substantial concentration of sources, with the UMS clustered around the (−0.6,−1.5) point and the red clump and RGB stars slightly to the right at (0,−1.5). To conservatively identify the YSOs, we define a horizontal line (F200W–F444W = −1.1) and a vertical line (F115W–F187N = 0.3) that enclose almost all of the UMS, red clump and RGB stars. In particular, the vertical line ensures that we are not including RGB stars with winds that may have a Paα excess.

A minority of sources appear to spread in the upper-right direction, roughly following our representative SMC reddening vector. In principle, these sources could be interpreted as either highly reddened objects due to their circumstellar material or as objects with substantial infrared excess, possibly associated with accretion emission in the F187N filter.

To break this degeneracy, we may look at the distribution of these outliers in the 2CD (Spatial distribution of NGC 346 stars). Examining the quadrants defined with respect to (0.3,−1.1), objects in the bottom-left quadrant are generally compatible with the main populations, with negligible reddening. Second, objects in the bottom-right quadrant (blue dots) have F200W–F444W compatible with stellar photospheres, but show a substantial F187N excess. One of these sources also showed Hα excess when observed with HST. Strong line emission in this case is the most viable explanation, with mass accretion, possibly a sporadic large episode, as a plausible source. In this case, the lack of F444W excess may suggest that the accreting disc has cleared its inner hot-dust component and accretion is supported largely by the gaseous phase. The spatial location of these objects in the NGC 346 field, several of them rather bright in the F115W filter, shows some concentration in correspondence with the brightest clumps of nebular emission. A notable fraction is spread in the field, however, suggesting that these accreting YSOs may be relatively evolved and dispersed. For simplicity, we refer to these objects as PMS objects.

Third, objects in the top-left quadrant (red squares), which we shall refer to as YSOs, have near-IR colours compatible with stellar photospheres and a substantial F444W excess, a characteristic incompatible with reddened objects. Of these, 29 also showed an Hα excess in the *HST* catalogue. These objects are clustered at the centre of the region but become more spread out in the southern part of our field. This latter grouping may be a candidate for transitional YSOs (that is, protoplanetary discs with inner holes in the dust distribution and negligible mass accretion).

Finally, the last class of objects (orange diamonds) is composed of sources in the top-right quadrant of the 2CD. In the F115W–F444W CMD, they appear well above the region occupied by low-mass MS and PMS stars, suggesting that they may be highly reddened, relatively massive stars. HST photometry indicates that 80 of these objects also show Hα excess. Their spatial distribution traces the main filaments of the region, suggesting that they are associated with ongoing star-formation sites. A large fraction of the accreting PMS stars detected by HST lie in this sector, supporting the hypothesis that these are bona fide YSOs that have not yet appreciably migrated from their birthplace. We shall refer to them as YSOs with Paα emission.

https://doi.org/10.1038/s41550-023-01945-7

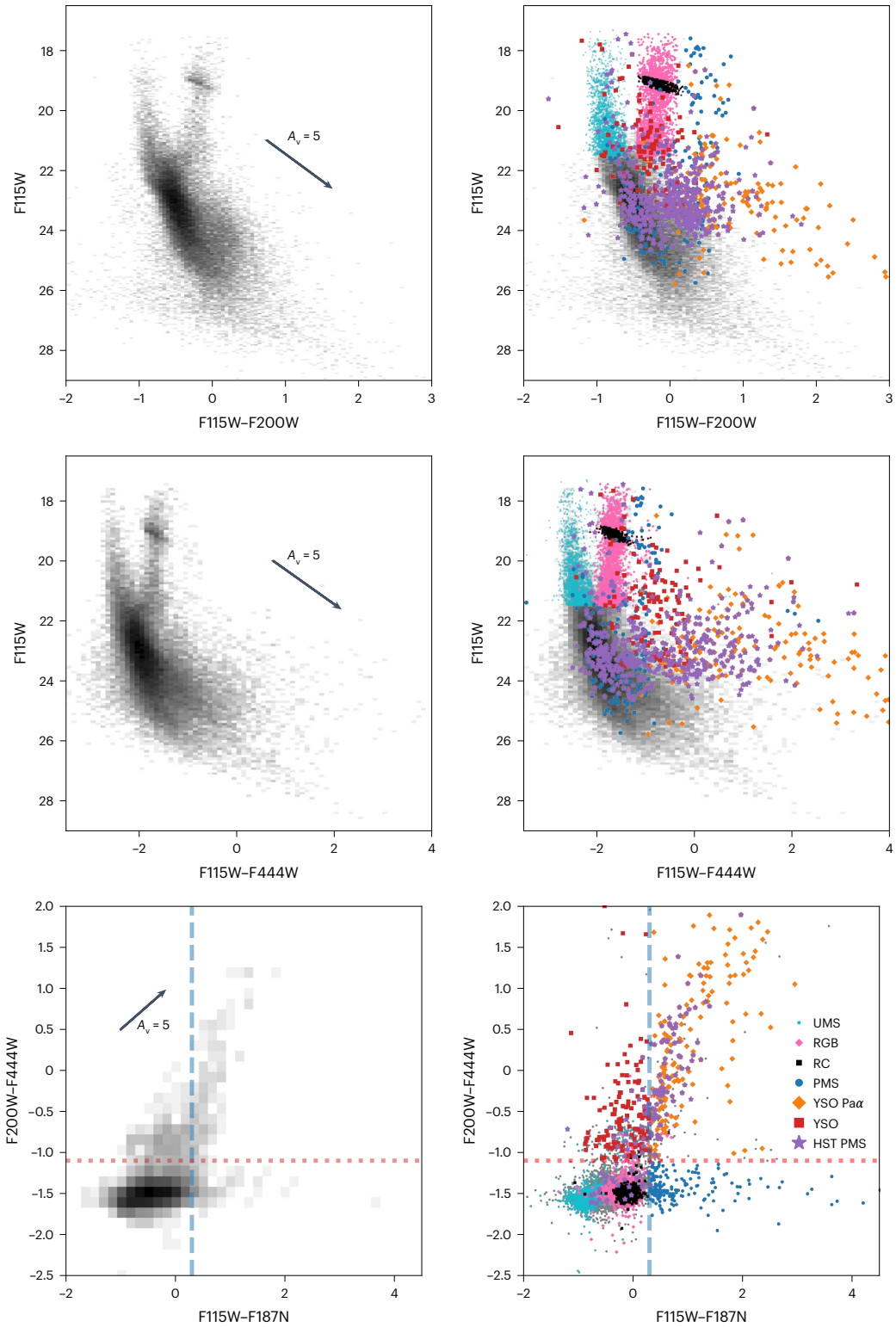


Fig. 2 | CMDs and colour–colour diagrams highlighting sources classified photometrically and as stellar density Hess diagrams for all point sources in the NGC 346 catalogue. Hess diagrams are shown on the left, while individual sources and their photometric classification are shown on the right. The RGB, red clump (RC), main-sequence turn-off and UMS are all easily identified in the stellar populations. In the bottom panels, the red dashed line separates sources with an infrared excess, whereas the blue dashed line separates objects with a Paα excess from the rest of the population.

This simplified, yet conservative selection of YSO and PMS candidates represents the deepest census of a star-forming region in a low-metallicity galaxy. Our data include redder candidates that are not present in HST optical catalogues because they are undetectable in those bands, as well as low-mass (roughly less than 2 $M_\odot$) sources significantly below the completeness limit of Spitzer surveys. Typically, YSOs in the early stages of formation can be completely obscured at optical wavelengths and faint in the near-infrared; however, the unprecedented

Table 1 | NGC 346 stellar populations identified using JWST/NIRCam (the stellar population, selection criteria and the resulting number of sources belonging to that class are listed below)

Population	Colour selection	Number of sources
RC	inside ($x1$,$y1$=(−0.45,18.8), $x2$,$y2$=(−0.45, 19.10), $x3$,$y3$=(0.10,19.55), $x4$,$y4$=(0.10,19.15)) where x=F115W and y=F115W–F200W	448
RGB	0.1>F115W–F200W>−0.45 and F115W<21.5	2,176
UMS	−0.6>F115W–F200W>−1.18 and F115W<21.5	1,982
YSO	F115W–F187N<0.3 and F200W–F444W>−1.1 and F335M–F444W>−0.3	136
YSO Paα	F115W–F187N>0.3 and F200W–F444W>−1.1 and F335M–F444W>−0.3	216
PMS	F115W–F187N>0.3 and F200W–F444W<−1.1	179

sensitivity of NIRCam enables the detection of sources with colours that are consistent with embedded low-mass YSOs, although additional mid-infrared data are necessary to assess the physical properties of the most embedded YSOs with ages younger than 0.1 Myr and to identify Class 0 sources, for example, ref. 46.

Spatial distribution of NGC 346 stars

Figure 1 shows there is a high degree of spatial overlap between YSOs (red squares), YSOs with Paα excess (orange diamonds) and the bright F444W dust emission. At optical wavelengths, many of these sources are either not visible (roughly 27%) or may be erroneously misidentified as main-sequence stars (De Marchi, in preparation), highlighting the importance of infrared observations to accurately interpret star-forming regions. We note that the location of both YSOs and YSOs with Paα excess do not necessarily correspond to the clusters previously identified in the HST data[16]. On the contrary, they tend to encircle the cavities created by the NGC 346 OB stars[35]. The distribution of the PMS stars and the newly identified YSOs supports the scenario proposed by ref. 34, in which a global hierarchical collapse culminates in 'river-like' structures responsible for the formation of clumps where significant changes in the coherence of the motion field are detected, and therefore where one expects high gas friction.

On the other hand, the older PMS stars (blue dots) that have cleared their dust envelopes and are optically thin are diffusely distributed across the field. This larger spatial dispersion is consistent with formation episodes over the past 20 Myr (refs. 18,47), and is probably due to both turbulent star formation and early dynamical evolution, in agreement with the spiralling nature and increasing rotation with distance from the centre of NGC 346, for example, refs. 11,34,35,47, due to hierarchical collapse[48].

As expected, we find that JWST surpasses the capability of Spitzer to detect candidate YSOs using only aperture photometry. This expands the observed sample of approximately 100 YSO candidates within NGC 346 by over a factor of three. Our survey reveals a population of dusty, subsolar mass YSOs and represents the deepest extragalactic census of these objects at low metallicity. The discovery of an associated infrared excess in these objects reveals substantial dust around low-mass YSOs in a 0.2 $Z_{\odot}$ extragalactic environment, suggesting that the material to form rocky planets is present at this low metallicity.

Methods

NIRCam observations and data processing

We have mapped NGC 346 with JWST/NIRCam (Program ID 1227; PI Meixner), in the F115W, F187N and F200W short-wavelength bands, and F277W, F335M and F444W long-wavelength bands. The images, obtained on 16 July 2022 are centred at right ascension of 00 h 59 min 04.9451 s, declination of −72° 10′ 9.15″ and cover an area of roughly 31.05 arcmin^2 (Table 2). The NIRCam observations used both the A and B modules to provide the largest field of view with one pointing. They were obtained in a four-by-four mosaic using the bright2 readout pattern with two groups per integration at four subpixel dither positions for an exposure time of 171.8 s per filter, for three of the tiles. The last tile was observed with seven groups per integration, to enable Mid-Infrared Instrument (MIRI) parallels, for a total exposure time of 601.3 s per filter.

Table 2 | Summary of the NGC 346 NIRCam survey, Guaranteed Time Program no. 1227 and values adopted for the properties of NGC 346 (the completeness limit corresponds to aperture photometry with a 1.5-pixel radius to 3σ)

Characteristic	Value
Nominal centre point	00 h 59 min 04.9451 s −72° 10′ 9.15″
Survey area (arcmin^2)	31.05
Central λ (μm)	1.154, 1.874, 1.990, 2.786, 3.365, 4.421
FWHM at λ (pixel)	1.290, 2.065, 2.129, 1.460, 1.762, 2.302
Point-source completeness limits at λ (mag)	26.6, 23.2, 26.7, 25.4, 24.5, 26.4
Maximum total exposure time per pixel	601.3 s
Distance to NGC 346	60.4 kpc
Distance modulus $(m-M)_0$	18.96 (ref. 1)
$E(B-V)$	0.08
Metallicity [Fe/H] (dex)	−0.9–1.0 Z=0.002

The level two NIRCam data were reprocessed using a slightly modified version of the JWST official pipeline (v.1.7.2). These modifications correct for 1/f noise (using image1overf.py; ref. 49), flat field correction noise, World Coordinate System alignment issues, differences in background matching across the mosaic and include the most recent NIRCam calibration files jwst_0989.map of the Operational Pipeline Calibration Reference Data System produced on 3 October 2022 with on-sky derived photometric zero points[50,51]. The final pixel scale of the mosaics is set to 0.0315″ for the three short-wavelength bands and 0.0629″ for the three long-wavelength bands.

Photometry

Aperture photometry was performed on the individual exposures in each band using the starbug II tool[52]. starbug II, which incorporates modules from photutils[53], is optimized for observations using both NIRCam and the MIRI[54] on JWST and is designed to detect and extract point sources in crowded environments with complex diffuse emission and variable backgrounds. The sources identified in the single frames are extracted at a 3σ level above the local background, which was characterized and globally subtracted using a combination of three different background estimation techniques. This ensures objects in complex nebular regions in which background determination is more problematic are not prematurely excluded. An aperture with radius 1.5 pixels and an annulus from 3.0 to 4.5 pixels surrounding each source was then used in the photometric extraction. Sharp cuts between 0.4 and 0.9 and round equal to or less than |1.0| are applied, and then only sources detected in at least three of the four frames are retained. Sources with mean and median values that differ by more than 0.1 dex between exposures were flagged and removed as mismatches. This eliminates cosmic rays, noise spikes from the point spread function and extended sources such as resolved background galaxies, and ensures high fidelity of the final point-source catalogues. Aperture corrections provided in the CRDS reference files were then applied to all photometry.

To generate a band-merged point-source catalogue, the individual catalogues from each of the six filters were merged using the closest astrometric separation less than 0.25″. Source blending/confusion is negligible (less than 3%) when combining between different filters. We correct the photometric values for galactic foreground extinction using $E(B-V) = 0.08$ and the extinction curve of ref. 55 with $R_V = 2.7$, but not for any extinction intrinsic to NGC 346. The final band-matched catalogue includes roughly 525,000 unique point sources, of which 45,583 are reliably detected in all four NIRCam wide bands. We refer to the latter sample as our NIRCam source catalogue, which we present in AB system magnitudes. Point sources in this catalogue have fewer nulled wavelengths, smaller photometric uncertainties and are typically brighter, thus less likely to have mismatched photometry when cross-matching with other telescopes (for example, HST, Gaia).

In the F115W band, the point-source completeness magnitude of 26.6 allows for the characterization of young populations (less than 10 Myr) down to an initial mass of roughly 0.1 $M_\odot$, corresponding to stars in the T-Tauri range. Sources brighter than F115W = 17.3 mag are saturated. To verify the PMS mass limits, we match (using $R < 0.3$″) our NIRCam catalogue to the refs. 29 and 18 HST data that include mass and age estimates. There are 24,367 sources in common, including PMS stars with masses from 0.4–4 $M_\odot$ and ages 1–30 Myr.

Data availability

The data used in this study may be obtained from the Mikulski Archive for Space Telescopes (MAST, https://mast.stsci.edu/) and are associated with program no. 1227.

Code availability

This research made use of astropy[56], photutils[53] and topcat[57]. The starbug II tool[52] optimized for JWST–NIRCam and MIRI point-source photometry in complex crowded environments is available via pip install starbug2.

References

1. de Grijs, R. & Bono, G. Clustering of local group distances: publication bias or correlated measurements? III. The Small Magellanic Cloud. *Astron. J.* **149**, 179 (2015).
2. Bouret, J. C. et al. Quantitative spectroscopy of O stars at low metallicity: O dwarfs in NGC 346. *Astrophys. J.* **595**, 1182–1205 (2003).
3. Peimbert, M., Peimbert, A. & Ruiz, M. T. The chemical composition of the Small Magellanic Cloud H II Region NGC 346 and the primordial helium abundance. *Astrophys. J.* **541**, 688–700 (2000).
4. Madau, P. & Dickinson, M. Cosmic star-formation history. *Annu. Rev. Astron. Astrophys.* **52**, 415–486 (2014).
5. Dimaratos, A., Cormier, D., Bigiel, F. & Madden, S. C. Modeling the physical properties in the ISM of the low-metallicity galaxy NGC 4214. *Astron. Astrophys.* **580**, A135 (2015).
6. Tchernyshyov, K. et al. Elemental depletions in the magellanic clouds and the evolution of depletions with metallicity. *Astrophys. J.* **811**, 78 (2015).
7. Roman-Duval, J. et al. Dust and gas in the Magellanic Clouds from the HERITAGE Herschel Key Project. II. Gas-to-dust ratio variations across interstellar medium phases. *Astrophys. J.* **797**, 86 (2014).
8. Johansen, A., Youdin, A. & Mac Low, M.-M. Particle clumping and planetesimal formation depend strongly on metallicity. *Astrophys. J. Lett.* **704**, L75–L79 (2009).
9. Li, R. & Youdin, A. N. Thresholds for particle clumping by the streaming instability. *Astrophys. J.* **919**, 107 (2021).
10. Ercolano, B. & Clarke, C. J. Metallicity, planet formation and disc lifetimes. *Mon. Not. R. Astron. Soc.* **402**, 2735–2743 (2010).
11. Cignoni, M., Tosi, M., Sabbi, E., Nota, A. & Gallagher, J. S. History and modes of star formation in the most active region of the Small Magellanic Cloud, NGC 346. *Astron. J.* **141**, 31 (2011).
12. Massey, P., Parker, J. W. & Garmany, C. D. The stellar content of NGC 346: a plethora of O stars in the SMC. *Astron. J.* **98**, 1305 (1989).
13. Evans, C. J., Lennon, D. J., Smartt, S. J. & Trundle, C. The VLT-FLAMES survey of massive stars: observations centered on the Magellanic Cloud clusters NGC 330, NGC 346, NGC 2004, and the N11 region. *Astron. Astrophys.* **456**, 623–638 (2006).
14. Dufton, P. L., Evans, C. J., Hunter, I., Lennon, D. J. & Schneider, F. R. N. A census of massive stars in NGC 346. *Astron. Astrophys.* **626**, A50 (2019).
15. Nota, A. et al. Discovery of a population of pre-main-sequence stars in NGC 346 from Deep Hubble Space Telescope ACS images. *Astrophys. J. Lett.* **640**, L29–L33 (2006).
16. Sabbi, E. et al. Past and present star formation in the SMC: NGC 346 and its neighborhood. *Astron. J.* **133**, 44–57 (2007).
17. Hennekemper, E., Gouliermis, D. A., Henning, T., Brandner, W. & Dolphin, A. E. NGC 346 in the Small Magellanic Cloud. III. Recent star formation and stellar clustering properties in the Bright H II Region N66. *Astrophys. J.* **672**, 914–929 (2008).
18. De Marchi, G., Panagia, N. & Sabbi, E. Clues to the star formation in NGC 346 across time and space. *Astrophys. J.* **740**, 10 (2011).
19. Bolatto, A. D. et al. The Spitzer survey of the Small Magellanic Cloud: S^3MC imaging and photometry in the mid- and far-infrared wave bands. *Astrophys. J.* **655**, 212–232 (2007).
20. Gordon, K. D. et al. Surveying the agents of galaxy evolution in the tidally stripped, low metallicity Small Magellanic Cloud (SAGE-SMC). I. Overview. *Astron. J.* **142**, 102 (2011).
21. Meixner, M. et al. The HERSCHEL inventory of the agents of galaxy evolution in the Magellanic Clouds, a Herschel Open Time Key program. *Astron. J.* **146**, 62 (2013).
22. Simon, J. D. et al. The Spitzer survey of the Small Magellanic Cloud: discovery of embedded protostars in the H II Region NGC 346. *Astrophys. J.* **669**, 327–336 (2007).
23. Sewiło, M. et al. Surveying the agents of galaxy evolution in the tidally stripped, low metallicity Small Magellanic Cloud (SAGE-SMC). III. Young Stellar Objects. *Astrophys. J.* **778**, 15 (2013).
24. Seale, J. P. et al. Herschel Key Program Heritage: a far-infrared source catalog for the Magellanic Clouds. *Astron. J.* **148**, 124 (2014).
25. Ruffle, P. M. E. et al. Spitzer infrared spectrograph point source classification in the Small Magellanic Cloud. *Mon. Not. R. Astron. Soc.* **451**, 3504–3536 (2015).
26. Rubio, M., Barbá, R. H. & Kalari, V. M. Massive Young Stellar Objects in the N 66/NGC 346 region of the SMC. *Astron. Astrophys.* **615**, A121 (2018).
27. Jones, O. C. et al. Near-infrared spectroscopy of embedded protostars in the massive metal-poor star forming region NGC 346. *Mon. Not. R. Astron. Soc.* **517**, 1518–1537 (2022).
28. Hony, S. et al. Star formation rates from young-star counts and the structure of the ISM across the NGC 346/N66 complex in the SMC. *Mon. Not. R. Astron. Soc.* **448**, 1847–1862 (2015).
29. Sabbi, E. et al. The Stellar Mass Distribution in the Giant Star Forming Region NGC 346. *Astron. J.* **135**, 173–181 (2008).
30. Gouliermis, D. A., Hony, S. & Klessen, R. S. The complex distribution of recently formed stars. Bimodal stellar clustering in the star-forming region NGC 346. *Mon. Not. R. Astron. Soc.* **439**, 3775–3789 (2014).
31. Rubio, M. et al. Multiwavelength observations of N 66 in the SMC: unveiling photodissociation interfaces and star formation. *Astron. Astrophys.* **359**, 1139–1146 (2000).
32. Contursi, A. et al. Mid-infrared imaging and spectrophotometry of N 66 in the SMC with ISOCAM. *Astron. Astrophys.* **362**, 310–324 (2000).
33. Neelamkodan, N. et al. ALMA reveals a cloud-cloud collision that triggers star formation in the Small Magellanic Cloud. *Astrophys. J. Lett.* **908**, L43 (2021).

34. Sabbi, E. et al. The internal proper motion kinematics of NGC 346: past formation and future evolution. *Astrophys. J.* **936**, 135 (2022).
35. Zeidler, P., Sabbi, E. & Nota, A. The internal line-of-sight kinematics of NGC 346: the rotation of the core region. *Astrophys. J.* **936**, 136 (2022).
36. Rieke, M. J., Kelly, D. & Horner, S. Overview of James Webb Space Telescope and NIRCam's role. In *Proc. Cryogenic Optical Systems and Instruments XI*, Vol. 5904 (eds Heaney, J. B. & Burriesci, L. G.) 1–8 (SPIE, 2005).
37. Bica, E. L. D. & Schmitt, H. R. A revised and extended catalog of Magellanic System Clusters, associations, and emission nebulae. I. Small Magellanic Cloud and bridge. *Astrophys. J. Suppl. Ser.* **101**, 41 (1995).
38. Rodríguez, M. J. et al. PHANGS-JWST first results: dust-embedded star clusters in NGC 7496 selected via 3.3 μm PAH emission. *Astrophys. J. Lett.* **944**, L26 (2023).
39. Dale, D. A. et al. PHANGS-JWST first results: the influence of stellar clusters on polycyclic aromatic hydrocarbons in nearby galaxies. *Astrophys. J. Lett.* **944**, L23 (2023).
40. Sandstrom, K. et al. PHANGS-JWST first results: mapping the 3.3 μm polycyclic aromatic hydrocarbon vibrational band in nearby galaxies with NIRCam medium bands. *Astrophys. J. Lett.* **944**, L7 (2023).
41. Lada, C. J. Peimbert, M. & Jugaku, J. (eds) in *Star Forming Regions* Vol. 115, 1–17 (IAU, 1987).
42. Robitaille, T. P., Whitney, B. A., Indebetouw, R., Wood, K. & Denzmore, P. Interpreting spectral energy distributions from Young Stellar Objects. I. A grid of 200,000 YSO model SEDs. *Astrophys. J. Suppl. Ser.* **167**, 256–285 (2006).
43. Whitney, B. A. et al. Spitzer Sage survey of the Large Magellanic Cloud. III. Star formation and˜ 1000 new candidate Young Stellar Objects. *Astron. J.* **136**, 18–43 (2008).
44. Gordon, K. D., Clayton, G. C., Misselt, K. A., Landolt, A. U. & Wolff, M. J. A quantitative comparison of the Small Magellanic Cloud, Large Magellanic Cloud, and Milky Way ultraviolet to near-infrared extinction curves. *Astrophys. J.* **594**, 279–293 (2003).
45. De Marchi, G. et al. Star formation in 30 Doradus. *Astrophys. J.* **739**, 27 (2011).
46. Jones, O. C., Meixner, M., Justtanont, K. & Glasse, A. Probing the dusty stellar populations of the local volume galaxies with JWST/MIRI. *Astrophys. J.* **841**, 15 (2017).
47. De Marchi, G. et al. Photometric determination of the mass accretion rates of pre-main-sequence stars. II. NGC 346 in the Small Magellanic Cloud. *Astrophys. J.* **740**, 11 (2011).
48. Vázquez-Semadeni, E., Palau, A., Ballesteros-Paredes, J., Gómez, G. C. & Zamora-Avilés, M. Global hierarchical collapse in molecular clouds. Towards a comprehensive scenario. *Mon. Not. R. Astron. Soc.* **490**, 3061–3097 (2019).
49. Willott, C. image1overf. *Github* https://github.com/chriswillott/jwst (2022).
50. Gordon, K. D. et al. The James Webb Space Telescope absolute flux calibration. I. Program design and calibrator stars. *Astron. J.* **163**, 267 (2022).
51. Boyer, M. L. et al. The JWST resolved stellar populations early release science program. I. NIRCam flux calibration. *Res. Notes Am. Astron. Soc.* **6**, 191 (2022).
52. Nally, C. & Jones, O. starbug2. *GitHub* https://github.com/conornally/starbug2 (2022).
53. Bradley, L. et al. astropy/photutils: 1.0.0. *Zenodo* https://doi.org/10.5281/zenodo.4044744 (2020).
54. Rieke, G. H. et al. The Mid-Infrared Instrument for the James Webb Space Telescope, I: introduction. *Publ. Astron. Soc. Pac.* **127**, 584 (2015).
55. Cardelli, J. A., Clayton, G. C. & Mathis, J. S. The relationship between infrared, optical, and ultraviolet extinction. *Astrophys. J.* **345**, 245–256 (1989).
56. Astropy Collaboration et al. Astropy: a community Python package for astronomy. *Astron. Astrophys.* **558**, A33 (2013).
57. Taylor, M. B., Shopbell, P., Britton, M. & Ebert, R. in *Astronomical Data Analysis Software and Systems XIV* Vol. 347 (eds Shopbell, P. et al.) (ASPC, 2005).

Acknowledgements

This work is based on observations made with the NASA/ESA/CSA JWST. The data were obtained from the Mikulski Archive for Space Telescopes at the Space Telescope Science Institute, which is operated by the Association of Universities for Research in Astronomy, Inc., under NASA contract no. NAS 5-03127 for JWST. These observations are associated with program no. 1227. O.C.J. acknowledges support from a Science and Technology Facilities Council Webb fellowship. K.F. acknowledges support through the ESA Research Fellowship. M.M. acknowledges support through a NASA/JWST grant no. 80NSSC22K0025. M.M., N.H. and L.L. acknowledge support from the National Science Foundation through grant no. 2054178. L.E.U.C. was supported by an appointment to the NASA Postdoctoral Program at the NASA Ames Research Center, administered by Oak Ridge Associated Universities under contract with NASA. O.N. acknowledges support from STScI Director's Discretionary Fund.

Author contributions

O.C.J. led the analysis and is the science lead of the NGC 346 Team. C.N. produced the photometric catalogues. N.H. and L.L. reprocessed the NIRCam data. K.F. and C.R. assisted in the photometry. M.R., G.d.M. and E.S. provided advice on NIRCam data processing and the analysis on comparison to HST data. L.E.U.C. produced images on NGC 346. A.S.H., M.M. and K.P. helped optimize the observations. All authors contributed to observation planning and/or scientific interpretation.

Competing interests

The authors declare no competing interests.

Additional information

Correspondence and requests for materials should be addressed to Olivia C. Jones.

Peer review information *Nature Astronomy* thanks the anonymous reviewers for their contribution to the peer review of this work.

Reprints and permissions information is available at www.nature.com/reprints.

Publisher's note Springer Nature remains neutral with regard to jurisdictional claims in published maps and institutional affiliations.

Springer Nature or its licensor (e.g. a society or other partner) holds exclusive rights to this article under a publishing agreement with the author(s) or other rightsholder(s); author self-archiving of the accepted manuscript version of this article is solely governed by the terms of such publishing agreement and applicable law.

© The Author(s), under exclusive licence to Springer Nature Limited 2023

[1]UK Astronomy Technology Centre, Royal Observatory, Edinburgh, UK. [2]Institute for Astronomy, University of Edinburgh, Edinburgh, UK. [3]Stratospheric Observatory for Infrared Astronomy, NASA Ames Research Center, Moffett Field, CA, USA. [4]European Space Research and Technology Centre, European Space Agency, Noordwijk, the Netherlands. [5]Space Telescope Science Institute, Baltimore, MD, USA. [6]NASA Postdoctoral Program Fellow, NASA Ames Research Center, Moffett Field, CA, USA. [7]Johns Hopkins University, Baltimore, MD, USA. [8]AURA for the European Space Agency, Space Telescope Science Institute, Baltimore, MD, USA. [9]ESAC, European Space Agency (ESA), Madrid, Spain. [10]INAF, Astronomical Observatory of Rome, Monteporzio Catone, Italy. [11]Leiden Observatory, Leiden University, Leiden, the Netherlands. [12]European Southern Observatory, Garching, Germany. ✉e-mail: olivia.jones@stfc.ac.uk